Biogeosciences Discuss., 12, 15223–15244, 2015
www.biogeosciences-discuss.net/12/15223/2015/
doi:10.5194/bgd-12-15223-2015
© Author(s) 2015. CC Attribution 3.0 License.

Biogeosciences Discussions
Open Access

This discussion paper is/has been under review for the journal Biogeosciences (BG).
Please refer to the corresponding final paper in BG if available.

Climate impacts on multidecadal pCO_2 variability in the North Atlantic: 1948–2009

M. L. Breeden and G. A. McKinley

Department of Atmospheric and Oceanic Sciences, University of Wisconsin – Madison, Wisconsin, USA

Received: 6 August 2015 – Accepted: 27 August 2015 – Published: 15 September 2015

Correspondence to: M. L. Breeden (mbreeden@wisc.edu)

Published by Copernicus Publications on behalf of the European Geosciences Union.

Abstract

The North Atlantic is the most intense region of ocean CO_2 uptake. Here, we investigate multidecadal timescale variability of the partial pressure CO_2 (pCO_2) that is due to the natural carbon cycle using a regional model forced with realistic climate and pre-industrial atmospheric pCO_2 for 1948–2009. Large-scale patterns of natural pCO_2 variability are primarily associated with basin-averaged sea surface temperature (SST) that, in turn, is composed of two parts: the Atlantic Multidecadal Oscillation (AMO) and a long-term positive SST trend. The North Atlantic Oscillation (NAO) drives a secondary mode of variability. For the primary mode, positive AMO and the SST trend modify pCO_2 with different mechanisms and spatial patterns. Warming with the positive AMO increases subpolar gyre pCO_2, but there is also a significant reduction of dissolved inorganic carbon (DIC) due primarily to reduced vertical mixing. The net impact of positive AMO is to reduce pCO2 in the subpolar gyre. Through direct impacts on SST, the net impacts of positive AMO is to increase pCO_2 in the subtropical gyre. From 1980 to present, long-term SST warming has amplified AMO impacts on pCO_2.

1 Introduction

To date, the ocean has removed approximately 1/3 of all anthropogenic carbon emitted to the atmosphere and has, thus, substantially damped climate warming (Khatiwala et al., 2009; Sabine et al., 2004). As carbon dioxide emissions continue to increase due to fossil fuel emissions and cement production, there is significant interest in better understanding the ocean carbon cycle. Due to the limited instrumental record and sparse data, multidecadal variability of the ocean carbon sink remains poorly constrained. The North Atlantic, in particular, is a region of highly concentrated carbon uptake (Takahashi et al., 2009) and of significant carbon cycle variability related to variations in the climate, often associated with the North Atlantic Oscillation (Fay and McKinley, 2013; Schuster et al., 2013; Terry, 2012; McKinley et al., 2011; Löptien and Eden, 2010;

BGD
12, 15223–15244, 2015

Ullman et al., 2009; Thomas et al., 2008). However, data are sparse, processes are complex and the timescales for studies have differed, and this has complicated a clear elucidation of the mechanisms of North Atlantic carbon cycle variations.

Schuster et al. (2009) analyzed in situ pCO_2 measurements, and suggested a substantial decline in North Atlantic carbon uptake from the mid-1990s to the mid-2000s. LeQuéré et al. (2010) also interpreted observations and models to conclude that there had been a decline in the North Atlantic sink from 1981–2007 due to changing wind patterns and increasing SST. Metzl et al. (2010) focused on subpolar surface ocean carbon cycle changes between 1993–2008, and also concluded that there had been a reduction in carbon uptake. In situ pCO_2 measurements have also been synthesized to illustrate the strong sensitivities of such changes to the locations and timeframe for the analyses (Fay and McKinley, 2013; McKinley et al., 2011). The substantial spatial heterogeneity and temporal variability in the North Atlantic complicates efforts to use sparse observations to quantify carbon uptake. Thus, the magnitude and mechanisms North Atlantic carbon cycle variability remains loosely constrained. The present study takes advantage of the full spatial and temporal coverage of a regional numerical model to gain new insights into the mechanisms of variability of North Atlantic pCO_2.

As shown by Ullman et al. (2009) in a 15 yr simulation (1992–2006), internal variability in the North Atlantic is partially obscured by the large, quasilinear trend of CO_2 flux into the ocean that is driven by increasing CO_2 emissions. To examine the carbon sink variability that is partially masked by this large carbon influx, we use a hindcast model from 1948–2009 forced with the preindustrial atmospheric CO_2 concentration and realistic climate. As described below, we find that the basin-average SST is associated with the leading mode of surface ocean pCO_2 variability. This SST signal, in turn, includes an upward trend due to greenhouse gas emissions and a signal of internal variability characterized by the Atlantic Multidecadal Oscillation (AMO, Kerr, 2000).

BGD
12, 15223–15244, 2015

2 Methodology

2.1 Physical-biogeochemical-ecosystem model

The MIT Ocean General Circulation Model (Marshall et al., 1997a,b) has been regionally configured for the North Atlantic between 20° S and 81.5° N (Bennington et al., 2009; Ullman et al., 2009). The model has a horizontal resolution of 0.5° latitude and 0.5° longitude and 23 vertical levels beginning with a resolution of 10 m thickness at the surface and increasing to 500 m thickness at depths greater than 2200 m. The Gent-McWilliams (Gent and McWilliams, 1990) eddy parameterization and the KPP boundary layer mixing scheme (Large et al., 1994) were employed to model sub-grid-scale processes. Daily fields from NCEP/NCAR Reanalysis I force the model from 1948–2009 (Kalnay et al., 1996). SST and SSS are relaxed to monthly historical SST (Had1SSTv1.0, Rayner et al., 2003) and climatological SSS (Antonov et al., 2006) observations, respectively. For tracers, a sponge layer was included along regional boundaries. The pelagic ecosystem is parameterized using one zooplankton class and two phytoplankton classes (diatoms and "small" phytoplankton) as described previously (Dutkiewicz et al., 2005; Bennington et al., 2009; Ullman et al., 2009). Carbon (inorganic and dissolved and particulate organic), alkalinity (ALK), phosphorus, silica and iron cycling are explicitly included in the biogeochemical model. Carbonate chemistry is modeled as in Follows et al. (2006). The objective of this simulation is to identify climate impacts on the natural carbon cycle without the complication of the large CO_2 flux into the ocean that is observed. Thus, atmospheric pCO_2 is fixed at a constant, preindustrial level of 278 ppmv.

The physical model was spun up for 100 yr. Following the physical spinup, the biogeochemical model was initialized using preindustrial estimates for DIC and ALK climatology from the GLODAP database (Key et al., 2004). The biogeochemical model was then spun up for an additional 60 yr, long enough to eliminate drift in the biogeochemical parameters. The model was then run with NCEP/NCAR daily forcing fields for 1948–2009.

BGD
12, 15223–15244, 2015

Model physics across the North Atlantic, as well as pCO_2, DIC and ALK at the Bermuda Atlantic Time Series (Bates, 2007) and in the subpolar North Atlantic have been compared to results from a previous simulation using with this same model forced with observed atmospheric pCO_2 for 1992–2006 (Ullman et al., 2009). These comparisons show that the model is capable of robustly simulating seasonality and trends in carbon biogeochemistry, and gives confidence in this pre-industrial simulation for which direct comparisons to carbon observations are not possible. Mikaloff-Fletcher et al. (2007) estimated the pre-industrial, or "natural", air-to-sea CO_2 flux in the North Atlantic with an ocean inversion that incorporated climatological circulations estimated from 10 ocean circulation models. For the North Atlantic from 0 to 75° N, they find an uptake of $0.27 \pm 0.07\,\mathrm{Pg\,C\,yr^{-1}}$. The mean natural CO_2 flux averaged over the same spatial domain in our simulation is consistent, $0.23\,\mathrm{Pg\,C\,yr^{-1}}$.

2.2 Post-processing

CO_2 flux into the ocean is proportional to the partial pressure difference between the atmosphere and ocean surface: $\Delta pCO_2 = pCO_2^{atm} - pCO_2^{ocn}$. In this analysis, we can directly relate higher pCO_2^{ocn} to a reduction in CO_2 flux, since atmospheric pCO_2 is fixed. ΔpCO_2 variability sets the sign and magnitude of flux changes on both seasonal and interannual timescales (Takahashi et al., 2009; Watson et al., 2009; LeQuéré et al., 2010). pCO_2 is decomposed into contributions from temperature and chemical effects using model output and the full carbonate equations (Follows et al., 2006). As in Ullman et al. (2009), pCO_2-SST is found by allowing only SST to vary in the full carbonate equations for pCO_2, i.e. all other variables (DIC, ALK, SSS, phosphate, silica) are held constant at their long-term mean values; pCO_2-chem is found by holding SST constant and allowing the rest of the input variables to vary; for pCO_2-DIC, only DIC varies.

Model diagnostics for DIC are the monthly mean tendency terms (in $\mathrm{mmol\,m^{-3}\,yr^{-1}}$) due to individual modeled processes and are calculated at each time step during the

BGD
12, 15223–15244, 2015

model simulation (Ullman et al., 2009). Monthly mean diagnostics for the surface layer DIC change due to horizontal and vertical advection and diffusion, net biological processes (primary production and respiration), freshwater input/removal, and air–sea CO_2 flux are used.

The AMO index for the model is calculated using modeled SST and observed global Had1SSTv1.0 (Rayner et al., 2003) using the approach of Wang and Dong (2010). This approach regresses the area-weighted global mean Had1SST time series onto area-weighted basin-wide mean North Atlantic SST time series (NASST). This regressed index is subtracted from the total NASST to define the AMO. The combined SST signal is, thus, decomposed into contributions from globally increasing SST (SST trend) and the internal variability of the AMO (Fig. 1d). In order to focus on the decadal timescale variability, all timeseries are smoothed with a standardized 121 month box smoother.

3 Results

3.1 Multidecadal variability

To determine the leading mode of variability in surface ocean pCO_2, principle component analysis is employed. The first empirical orthogonal function (EOF1) patterns and smoothed principle components (PCs) for monthly, 13 month smoothed total pCO_2 and the SST contribution to pCO_2 (pCO_2-SST) are shown in Fig. 1a–c. To determine the change in pCO_2 anomalies described by EOF1 at a specific point in time, the value of the PC1 at that time can be multiplied by the EOF1 pattern. The percent of variance in the total field explained by the EOF1 pattern is 18 and 38 % for pCO_2 and pCO_2-SST, respectively. In both cases, the EOF1 patterns are statistically distinct from their EOF2 patterns, which are discussed in Sect. 4. This EOF analysis unveils the basin-scale coherent variability. There is remaining variability in coherent secondary large-scale modes (e.g. EOF2) or at scales smaller than the whole basin. That large-scale modes of climatic variability tend to capture 10–40 % of variance has been documented across

BGD
12, 15223–15244, 2015

many climate variables, including global SST and tropospheric winds (von Storch and Zwiers, 1999), Southern Ocean geopotential heights (Thomson and Wallace, 2000), and pCO_2 throughout the Pacific (McKinley et al., 2004, 2006). That pCO_2 EOF1 captures the patterns of multi-decadal large-scale change is further evidenced by plots of 20 yr anomalies of pCO_2 (Fig. S1).

The correlation between PC1-pCO_2 and the area-weighted basin-averaged SST is 0.88 (Fig. 1c, Table S1). An increase in temperature increases pCO_2 by reducing solubility, which is illustrated by the pCO_2-SST EOF1 pattern. As expected, PC1-pCO_2-SST is highly correlated (r = 1.0) with SST itself (Fig. 1c, Table S1).

PC1-pCO_2 and PC1-pCO_2-SST are highly correlated (Fig. 1c, r = 0.91), but have distinct EOF1 patterns, particularly in the subpolar gyre (Fig. 1a and b). This is because pCO_2 in the subpolar gyre is also significantly impacted by DIC variability that, in turn, is associated with the AMO. EOF1 for pCO_2-chem and pCO_2-DIC explain 32 and 25 % of the variance, respectively (Fig. 2a and b), and their PC1's are highly correlated with the AMO, r = 0.99, 0.96, respectively (Fig. 2c, Table S1). The AMO, an index of internal North Atlantic SST variability, declines (cools) until 1975 and rises thereafter (Fig. 1d). Taking the last half of the timeseries as an example, increasingly positive AMO corresponds to a decrease in pCO_2-chem, with the strongest declines in the subpolar gyre and driven by reduced pCO_2-DIC (Fig. 2). This occurs in opposition to the direct effect on pCO_2 of warmer NASST (Fig. 1b and c), driven jointly by the increasingly positive AMO and the warming trend (Fig. 1d). SST and chemical terms vary inversely because higher SST enhances stratification, leading to a shoaling of mixed layer depths over most of the gyre (Fig. S2). This shoaling in turn limits the amount of deep, carbon-rich water that is mixed to the surface, reducing pCO_2-DIC and pCO_2-chem (Ullman et al., 2009). The correlation of PC1-pCO_2-chem and PC1-pCO_2-DIC with PC1-pCO_2-SST are 0.90 and 0.91, respectively (Table S1). Mechanisms of AMO impacts on pCO_2-chem in the subpolar gyre will be explored further below.

BGD
12, 15223–15244, 2015

3.2 Regression analysis

Regression of the AMO, SST trend, and total SST (Fig. 1d) onto monthly pCO_2, pCO_2-SST and pCO_2-chem further illustrates that temperature and chemical responses tend to act in opposition to one another, damping total pCO_2 responses across the basin (Fig. 3). Previous studies with observations and models have shown that the pCO_2-chem dominates the seasonality of pCO_2 in the subpolar gyre, via strong vertical supply of DIC in winter that drives up pCO_2 and biological DIC drawdown in summer that drives pCO_2 down. Temperature impacts oppose these seasonal oscillations, but are of weaker amplitude (Kortzinger et al., 2008; Takahashi et al., 2002). Models have shown similar opposing influences with respect to interannual variability (Ullman et al., 2009; McKinley et al., 2004). These regressions illustrate that positive AMO leads to higher pCO_2-SST throughout the basin (Fig. 3b). The response is strongest north of 35° N with a clear maximum to the east of Newfoundland. Simultaneously, positive AMO is associated with a reduction in pCO_2-chem (Fig. 3c). The pCO_2-chem signal is also strongest to the north. The overall effect is a decrease in total pCO_2 north of 45° N and a slight increase in pCO_2 in the eastern subtropical gyre (Fig. 3a).

When responding to the global SST trend, pCO_2-SST more heavily controls the response of the total pCO_2 field (Fig. 3d and e). The pCO_2-SST response is strongest along the Gulf Stream and east of Newfoundland, and also increases somewhat off the coast of Europe and Africa. pCO_2-chem exhibits some decline in the Gulf Stream region, and has a small response elsewhere (Fig. 3f).

Regression with the total NASST timeseries (Fig. 1) illustrates the combined effects of the AMO and trend signals (Fig. 3g–i). A positive anomaly of NASST depresses total pCO_2 in the subpolar gyre, consistent with the AMO impact found above. Positive NASST also increases total pCO_2 off North Africa, consistent with the impact of the SST trend. pCO_2-SST increases both off Africa and has a strong maximum in the Gulf Stream region east of Newfoundland with positive NASST anomlies. The pCO_2-chem response is slightly weaker in the subpolar gyre than for the AMO alone (Fig. 3a and i).

BGD
12, 15223–15244, 2015

3.3 DIC diagnostics

To further investigate the chemical term response to the AMO, model diagnostics for the DIC field are regressed upon the AMO index. Diagnostics are modeled rates of change in DIC due to one of five processes that have been saved at every model time-step. Physical processes are separated into horizontal advection and diffusion (DIC-horz), and vertical advection and diffusion (DIC-vert). DIC-phys is the sum of vertical and horizontal transport, showing the net effect of physical transport on DIC (Fig. 4). The rate of DIC supply is also affected by biological processes involving DIC deposition and remineralization (DIC-bio), net precipitation/evaporation that dilutes or concentrates DIC (DIC-fresh) and the air–sea flux of CO_2 (DIC-flx) (Fig. 5). The focus on DIC is justified by the fact that pCO_2-chem change has the same pattern and is highly correlated with pCO_2-DIC change (Fig. 2). The focus on the AMO is justified by its strong imprint on pCO_2 through pCO_2-chem (Figs. 2 and 3).

For the long-term average, vertical advection and diffusion are positive along the Gulf Stream and in the subpolar gyre due to deep winter mixed layer depths (MLD) that mix up high-DIC water from below (Fig. 4a). Horizontal DIC advection and mixing removes this vertically supplied DIC along the Gulf Stream and in the western subpolar gyre (Fig. 4b). While the vertical and horizontal components tend to have opposing influences, the net effect is a positive DIC supply to the subpolar gyre, as shown by mean DIC-phys (Fig. 4c). With positive AMO, vertical advective and diffusive fluxes of DIC decrease in the Irminger Sea and Iceland basin, while they increase in the Labrador Sea and east of Newfoundland (Fig. 4d). These changes are consistent with AMO-related MLD changes outside of the Labrador Sea (Fig. S2) and change in the basin-scale barotropic streamfunction indicating a weakened subpolar gyre (Fig. S3). The effect of this is to shift the central DIC-vert maximum to the west. With positive AMO, horizontal advection and diffusion largely respond to changes in vertical advection and diffusion, with less horizontal divergence (a positive change) in regions where the vertical supply is reduced (Fig. 4e). The net effect shown by DIC-phys reveals an overall reduction in

BGD
12, 15223–15244, 2015

DIC supply (Fig. 4f), consistent with a weaker subpolar gyre circulation and shallower MLDs that reduce the vertical supply of DIC. Hakkinen and Rhines (2009) illustrate and increased penetration of subtropical waters into the subpolar region from the 1990s to the 2000s, consistent with a weaker subpolar gyre circulation.

Mean DIC impacts from physics, biological processes, freshwater and air–sea flux are shown in Fig. 5a–e. The net impact of biology is to remove DIC from the surface of most of the region, with the most intense removal along the Gulf Stream (Fig. 5a). The smaller impact of evaporation and precipitation is to concentrate DIC in the subtropics and to dilute it in the subpolar gyre (Fig. 5b). The air–sea CO_2 flux term is also small, positive north of about 35° N and negative to the south (Fig. 5c). AMO-related change in the biological removal of DIC indicates additional removal (negative anomaly) occurring in the same region where horizontal flux increases, consistent with biological stimulation through an increased supply nutrients from the subtropical subsurface along the "nutrient stream" (Williams et al., 2006). There is reduced biological productivity, and thus a reduction of DIC loss (a positive DIC anomaly), in other parts of the basin that are consistent with satellite observations from the late 1990s to the mid-2000s (Behrenfeld et al., 2006). Changes in surface ocean DIC content due to freshwater fluxes and air–sea CO_2 flux with the AMO are small. Across the basin, the net DIC change associated with AMO is negative, with the strongest negative changes occurring in the subpolar gyre (Figs. 2b and 3c).

4 Discussion and conclusions

In this North Atlantic regional model forced with pre-industrial pCO_2 and realistic climate from 1948–2009, SST is the dominant driver of pCO_2 variability, with both long-term anthropogenic warming and the AMO playing important roles. The AMO is strongly associated with chemical change, which in turn is mostly driven by DIC. DIC changes, in turn, are due primarily to changes in vertical and horizontal advection and mixing. Changing biology has the most important secondary effect, and largely damps

BGD
12, 15223–15244, 2015

the anomalies caused by advection and mixing. Freshwater and CO_2 fluxes changes are slight.

Our findings linking the AMO to natural carbon cycle variability in the North Atlantic are consistent with the study of Séférian et al. (2013) who also found an AMO-like signal dominated North Atlantic pCO_2 variability in a 1000 yr Earth System Model simulation with constant pCO_2. Other studies have focused on the relationship between the North Atlantic Oscillation (NAO) and CO_2 flux using models and observations (Löptien and Eden, 2010; Ullman et al., 2009; Schuster et al., 2009; Thomas et al., 2008). Consistent with these previous studies, the NAO is the second mode of variability in this simulation (Figs. S4 and S5), and the corresponding principle components are highly correlated with the NAO (Table S2). The shorter timeframe for most previous studies explains, in part, the difference in attribution to the AMO as opposed to NAO. Our results are broadly consistent with previous studies in the finding that physical variability is the dominant driver of variability in the North Atlantic surface ocean carbon cycle.

The NAO and AMO may, in fact, be linked through the Meridional Overturning Circulation (MOC), with a positive NAO enhancing MOC, which over time warms SSTs and leads to a positive AMO. The precise mechanisms remain in debate due to different model findings and a lack of observational constraints (Delworth and Mann, 2000; Knight et al., 2005; Dima and Lohmann, 2007; Latif et al., 2006). In this simulation, the NAO and MOC are significantly correlated (r = 0.57, Table S1) and there is also a high correlation (r = 0.86) between the NAO (Fig. S3) and the 15 yr lagged AMO. These correlations are consistent with the above-postulated NAO-MOC-AMO relationship. Future modeling and observations should further elucidate these connections.

We find multidecadal variability in the natural carbon cycle of the surface North Atlantic to be dominated by the SST trend and multidecadal SST variation captured by the AMO index. Variability linked to AMO influences both pCO_2-SST and pCO_2-chem. In the subpolar gyre, the positive SST influence on pCO_2 is overwhelmed by reduced supply of DIC to the surface ocean through mixing and advection, the net impact being reduced pCO_2. The reduction in mixing is associated with shoaling of MLDs and

BGD
12, 15223–15244, 2015

a weaker subpolar gyre circulation, both associated with warmer SSTs (positive AMO). In the subtropics, the SST impact is stronger and thus pCO_2 is increased under the influence of positive AMO and positive SST trend.

These findings are consistent with observed relationships between trends in surface ocean pCO_2 and trends in atmospheric pCO_2 since the 1980s (Fay and McKinley, 2013). In the North Atlantic subpolar gyre, trends in surface ocean pCO_2 lagged the trend in atmospheric pCO_2 from the early to mid 1990s to the late 2000s, which is consistent with the AMO and the SST trend reducing DIC supply to the subpolar gyre as found in this study. On smaller spatial scales and shorter timeframes, trends in ocean pCO_2 can differ (Fay and McKinley, 2013; Metzl, 2010; Watson et al., 2009; Schuster et al., 2009), which can be reasonably attributed to shorter-term and smaller spatial scale variability. We also find that warming has contributed to the observed pCO_2 increase from the 1980–1990s through the 2000s throughout the basin. These model results allow a mechanistic attribution of these observed changes in North Atlantic pCO_2 to the combined effect of the AMO and a positive SST trend due to anthropogenic climate change.

The Supplement related to this article is available online at doi:10.5194/bgd-12-15223-2015-supplement.

Acknowledgements. The authors are grateful for support from NASA grants (NNX/11AF53G, and NNX/13AC53G). Model code is freely available at MITgcm.org; model fields analyzed here can be acquired by contacting GAM.

References

Antonov, J. I., Locarnini, R. A., Boyer, T. P., Mishonov, A. V., and Garcia, H. E.: World Ocean Atlas 2005 Vol. 2, Salinity, NOAA Atlas NESDIS 62, edited by: Levitus, S., US Govt. Print. Off., Washington, DC, 182 pp., 2006.

BGD
12, 15223–15244, 2015

Bates, N. R.: Interannual variability of the oceanic CO_2 sink in the subtropical gyre of the North Atlantic Ocean over the last 2 decades, J. Geophys. Res., 112, C09013, doi:10.1029/2006JC003759, 2007.
Behrenfeld, M. J., O'Malley, R. T., Siegel, D. A., McClain, C. R., Sarmiento, J. L., Feldman, G. C., Milligan, A. J., Falkowski, P. G., Letelier, R. M., and Boss, E. S.: Climate-driven trends in contemporary ocean productivity, Nature, 444, 752–755, 2006.
Bennington, V., McKinley, G. A., Dutkiewicz, S., and Ullman, D.: What does chlorophyll variability tell us about export and CO_2 flux variability in the North Atlantic?, Global Biogeochem. Cy., 23, GB3002, doi:10.1029/2008GB003241, 2009.
Delworth, T. L. and Mann, M. E.: Observed and simulated multidecadal variability in the Northern Hemisphere, Clim. Dynam., 16, 661–676, doi:10.1007/s003820000075, 2000.
Dima, M. and Lohmann, G.: A hemispheric mechanism for the Atlantic Multidecadal Oscillation, J. Climate, 20, 2706–2718, doi:10.1175/JCLI4174.1, 2007.
Dutkiewicz, S., Follows, M. J., and Parekh, P.: Interactions of the iron and phosphorus cycles: a three-dimensional model study, Global Biogeochem. Cy., 19, GB1021, doi:10.1029/2004GB002342, 2005.
Fay, A. R. and McKinley, G. A.: Global trends in surface ocean pCO_2 from in situ data, Global Biogeochem. Cy., 27, 541–557, doi:10.1002/gbc.20051, 2013.
Follows, M. J., Dutkiewicz, S., and Ito, T.: On the solution of the carbonate system in ocean biogeochemistry models, Ocean Model., 12, 290–301, doi:10.1016/j.ocemod.2005.05.004, 2006.
Gent, P. R. and McWilliams, J. C.: Isopycnal mixing in ocean general circulation models, J. Phys. Oceanogr., 20, 150–155, 1990.
Hakkinen, S. and Rhines, P. B.: Shifting surface currents in the northern North Atlantic Ocean, J. Geophys. Res., 114, C04005, doi:10.1029/2008JC004883, 2009.
Key, R. M., Key, R. M., Kozyr, A., Sabine, C. L., Lee, K., Wanninkhof, R., Bullister, J. L., Feely, R. A., Millero, F. J., Mordy, C., and Peng T.-H.: A global ocean carbon climatology: results from Global Data Analysis Project (GLODAP), Global Biogeochem. Cy., 18, GB4031, doi:10.1029/2004GB002247, 2004.
Kalnay, E., Kanamitsu, M., Kistler, R., Collins, W., Deaven, D., Gandin, L., Iredell, M., Saha, S., White, G., Woollen, J., Zhu, Y., Leetmaa, A., Reynolds, R., Chelliah, M., Ebisuzaki, W., Higgins, W., Janowiak, J., Mo, K. C., Ropelewski, C., Wang, J., Jenne, R., and Joseph, D.:

BGD
12, 15223–15244, 2015

The NCEP/NCAR 40-Year Reanalysis Project, B. Am. Meteorol. Soc., 77, 437–471, doi:10.1175/1520-0477(1996)077<0437:TNYRP>2.0.CO;2, 1996.
Kerr, R. A.: A North Atlantic climate pacemaker for the centuries, Science, 288, 1984–1985, doi:10.1126/science.288.5473.1984, 2000.
Khatiwala, S., Primeau, F., and Hall, T.: Reconstruction of the history of anthropogenic CO_2 concentrations in the ocean, Letters to Nature, 462, 346–349, doi:10.1038/nature08526, 2009.
Knight, J. R., Allan, R. J., Folland, C. K., Vellinga, M., and Mann, M. E.: A signature of persistent natural thermohaline circulation cycles in observed climate, Geophys. Res. Lett., 32, L20708, doi:10.1029/2005GL024233, 2005.
Körtzinger, A., Send, U., Lampitt, R. S., Hartman, S., Wallace, D. W. R., Karstensen, J., Villagarcia, M. G., Llinás, O., and DeGrandpre, M. D.: The seasonal pCO_2 cycle at 49° N/16.5° W in the northeastern Atlantic Ocean and what it tells us about biological productivity, J. Geophys. Res., 113, C04020, doi:10.1029/2007JC004347, 2008.
Large, W. G., McWilliams, J. C., and Doney, S. C.: Oceanic vertical mixing: a review and a model with a nonlocal boundary layer parameterization, Rev. Geophys., 32, 363–403, 1994.
Latif, M., Böning, C., Willebrand, J., Biastoch, A., Dengg, J., Keenlyside, N., Schweckendiek, U., and Madec, G.: Is the thermohaline circulation changing?, J. Climate, 19, 4631–4637, doi:10.1175/JCLI3876.1, 2006.
Le Quéré, C., Takahashi, T., Buitenhuis, E. T., Rödenbeck, C., and Sutherland, S. C.: Impact of climate change and variability on the global oceanic sink of CO_2, Global Biogeochem. Cy., 24, GB4007, doi:10.1029/2009GB003599, 2010.
Löptien, U. and Eden, C.: Multidecadal CO_2 uptake variability of the North Atlantic, J. Geophys. Res., 115, D12113, doi:10.1029/2009JD012431, 2010.
Marshall, J. C., Adcroft, A., Hill, C., Perelman, L., and Heisey, C.: A finite volume, incompressible Navier–Stokes model for studies of the ocean on parallel computers, J. Geophys. Res., 102, 5753–5766, 1997a.
Marshall, J. C., Hill, C., Perelman, L., and Adcroft, A.: Hydrostatic, quasi-hydrostatic and nonhydrostatic ocean modeling, J. Geophys. Res., 102, 5733–5752, 1997b.
McKinley, G. A., Follows, M. J., and Marshall, J.: Mechanisms of air–sea CO_2 flux variability in the equatorial Pacific and the North Atlantic, Global Biogeochem. Cy., 18, GB2011, doi:10.1029/2003GB002179, 2004.
McKinley, G. A., Takahashi, T., Buitenhuis, E., Chai, F., Christian, J. R., Doney, S. C., Jiang, M.-S., Lindsay, K., Moore, J. K., Le Quéré, C., Lima, I., Murtugudde, R., Shi, L., and Wetzel, P.:

BGD
12, 15223–15244, 2015

North Pacific carbon cycle response to climate variability on seasonal to decadal timescales, J. Geophys Res.-Oceans, 111, C07S06, doi:10.1029/2005JC003173, 2006.
McKinley, G. A., Fay, A. R., Takahashi, T., and Metzl, N.: Convergence of atmospheric and North Atlantic carbon dioxide trends on multidecadal timescales, Nat. Geosci., 4, 606–610, doi:10.1038/Ngeo1193, 2011.
Metzl, N., Corbière, A., Reverdin, G., Lenton, A., Takahashi, T., Olsen, A., Johannessen, T., Pierrot, D., Wanninkhof, R., Ólafsdóttir, S. R., Olafsson, J., and Ramonet, M.: Recent acceleration of the sea surface fCO_2 growth rate in the North Atlantic subpolar gyre (1993–2008) revealed by winter observations, Global Biogeochem. Cy., 24, GB4004, doi:10.1029/2009GB003658, 2010.
Mikaloff Fletcher, S. E., Gruber, N., Jacobson, A. R., Gloor, M., Doney, S. C., Dutkiewicz, S., Gerber, M., Follows, M., Joos, F., Lindsay, K., Menemenlis, D., Mouchet, A., Müller, S. A., and Sarmiento, J. L.: Inverse estimates of the oceanic sources and sinks of natural CO_2 and the implied oceanic carbon transport, Global Biogeochem. Cy., 21, GB1010, doi:10.1029/2006GB002751, 2007.
Rayner, N. A., Parker, D. E., Horton, E. B., Folland, C. K., Alexander, L. V., Rowell, D. P., Kent, E. C., and Kaplan, A.: Global analyses of sea surface temperature, sea ice, and night marine air temperature since the late nineteenth century, J. Geophys. Res., 108, 4407, doi:10.1029/2002JD002670, 2003.
Sabine, C. L., Feely, R. A., Gruber, N., Key, R. M., Lee, K., Bullister, J. L., Wanninkhof, R., Wong, C. S., Wallace, D. W. R., Tilbrook, B., Millero, F. J., Peng, T., Kozyr, A., Ono, T., and Rios, A. F.: The oceanic sink for anthropogenic CO_2, Science, 305, 367–371, doi:10.1126/science.1097403, 2004.
Schuster, U., Watson, A. J., Bates, N., Corbière, A., González-Dávila, M., Metzl, N., Pierrot, D., and Santana-Casiano, J. M.: Trends in North Atlantic sea-surface fCO_2 from 1990 to 2006, Deep-Sea Res. II, 56, 620–629, doi:10.1016/j.dsr2.2008.12.011, 2009.
Schuster, U., McKinley, G. A., Bates, N., Chevallier, F., Doney, S. C., Fay, A. R., González-Dávila, M., Gruber, N., Jones, S., Krijnen, J., Landschützer, P., Lefèvre, N., Manizza, M., Mathis, J., Metzl, N., Olsen, A., Rios, A. F., Rödenbeck, C., Santana-Casiano, J. M., Takahashi, T., Wanninkhof, R., and Watson, A. J.: An assessment of the Atlantic and Arctic sea–air CO_2 fluxes, 1990–2009, Biogeosciences, 10, 607–627, doi:10.5194/bg-10-607-2013, 2013.

BGD
12, 15223–15244, 2015

Séférian, R., Bopp, L., Swingedouw, D., and Servonnat, J.: Dynamical and biogeochemical control on the decadal variability of ocean carbon fluxes, Earth Syst. Dynam., 4, 109–127, doi:10.5194/esd-4-109-2013, 2013.

Takahashi, T., Sutherland, S. C., Sweeney, C., Poisson, A., Metzl, N., Tilbrook, B., Bates, N., Wanninkhof, R., Feely, R. F., Sabine, C., Olafsson, J., and Nojiri, Y.: Global sea–air CO_2 flux based on climatological surface ocean pCO_2, and seasonal biological and temperature effects, Deep-Sea Res. II, 49, 1601–1622, 2002.

Takahashi, T., Sutherland, S. C., Wanninkhof, R., Sweeney, C., Feely, R. A., Chipman, D. W., Hales, B., Friederich, G., Chavez, F., Sabine, C., Watson, A., Bakker, D. C. E., Schuster, U., Metzl, N., Yoshikawa-Inoue, H., Ishii, M., Midorikawa, T., Nojiri, Y., Körtzinger, A., Steinhoff, T., Hoppema, M., Olafsson, J., Arnarson, T. S., Tilbrook, B., Johannessen, T., Olsen, A., Bellerby, R., Wong, C. S., Delille, B., Bates, N. R., and de Baar, H. J. W.: Climatological mean and decadal change in surface ocean pCO_2, and net sea–air CO_2 flux over the global oceans, Deep-Sea Res. II, 56, 554–577, doi:10.1016/j.dsr2.2008.12.009, 2009.

Terry, L.: Evidence for multiple drivers of North Atlantic multi-decadal climate variability, Geophys. Res. Lett., 39, L19712, doi:10.1029/2012GL053046, 2012.

Thomas, H. F., Prowe, A. E., Lima, I. D., Doney, S. C., Wanninkhof, R., Greatbatch, R. J., Schuster, U., and Corbière, A.: Changes in the North Atlantic oscillation influence CO_2 uptake in the North Atlantic over the past 2 decades, Global Biogeochem. Cy., 22, GB4027, doi:10.1029/2007GB003167, 2008.

Thompson, D. and Wallace, J. M.: Annular modes in the extratropical circulation, Part I: Month-to-month variability, J. Climate, 13, 1000–1016, 2000.

Ullman, D. J., McKinley, G. A., Bennington, V., and Dutkiewicz, S.: Trends in the North Atlantic carbon sink: 1992–2006, Global Biogeochem. Cy., 23, GB4011, doi:10.1029/2008GB003383, 2009.

Von Storch, H. and Zwiers, F. W.: Statistical Analysis in Climate Research, Cambridge University Press., 484 pp., 1999.

Wang, C. and Dong, S.: Is the basin-wide warming in the North Atlantic Ocean related to atmospheric carbon dioxide and global warming?, Geophys. Res. Lett., 37, L08707, doi:10.1029/2010GL042743, 2010.

Watson, A. J., Schuster, U., Bakker, D. C. E., Bates, N. R., Corbière, A., González-Dávila, M., Friedrich, T., Hauck, J., Heinze, C., Johannessen, T., Körtziner, A., Metzl, N., Olafsson, J., Olsen, A., Oschlies, A., Padin, X. A., Pfeil, B., Santana-Casiano, J. M., Steinhoff, T., Tel-

BGD
12, 15223–15244, 2015

szewski, M., Rios, A. F., Wallace, D. W. R., and Wanninkhof, R.: Tracking the variable North Atlantic sink for atmospheric CO_2, Science, 326, 1391–1393, doi:10.1126/science.1177394, 2009.

Williams, R. G., Roussenov, V., and Follows, M. J.: Induction of nutrients into the mixed layer and maintenance of high latitude productivity, Global Biogeochem. Cy., 20, GB1016, doi:10.1029/2005GB002586, 2006.

BGD
12, 15223–15244, 2015

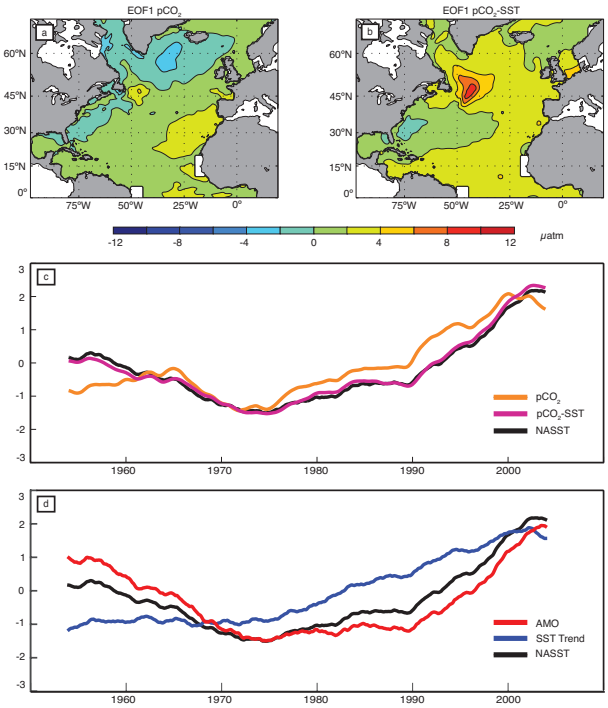

Figure 1. (a) EOF1 of total pCO_2 (µatm), **(b)** EOF1 of pCO_2-SST (µatm), explaining 18 and 38 % of total variance, respectively. **(c)** PC1-pCO_2 (orange), PC1-pCO_2-SST (pink) and area-weighted, basin-averaged standardized North Atlantic SST time series (black), **(d)** Area-weighted, basin-averaged (0–70° N, 98° W–19.5° E) North Atlantic SST from Had1SST (black), global area-weighted SST regressed onto North Atlantic SST (blue), and AMO index created by subtracting the global regression from the North Atlantic SST (red). All indices are standardized by 1 sigma. Timeseries smoothed with a 121 month box smoother. Two small coastal areas off Africa and South America were excluded in **(a)** and **(b)** due to the presence of localized, anomalously strong upwelling in the early 1960's that precluded elucidation of the large-scale pattern.

BGD
12, 15223–15244, 2015

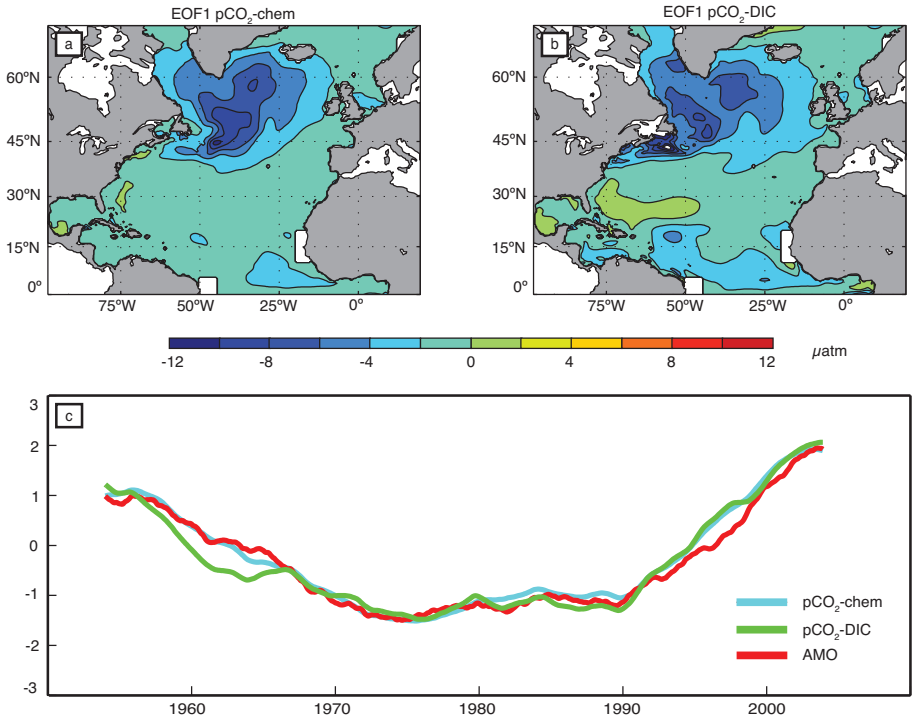

Figure 2. (a) EOF1 pCO_2-chem (µatm), **(b)** EOF1 pCO_2-DIC (µatm), explaining 32 and 25 % of total variance, respectively, **(c)** PC1-pCO_2-chem (cyan), PC1-pCO_2-DIC (green) and AMO index (red), all standardized. Timeseries smoothed with a 121 month box smoother.

BGD
12, 15223–15244, 2015

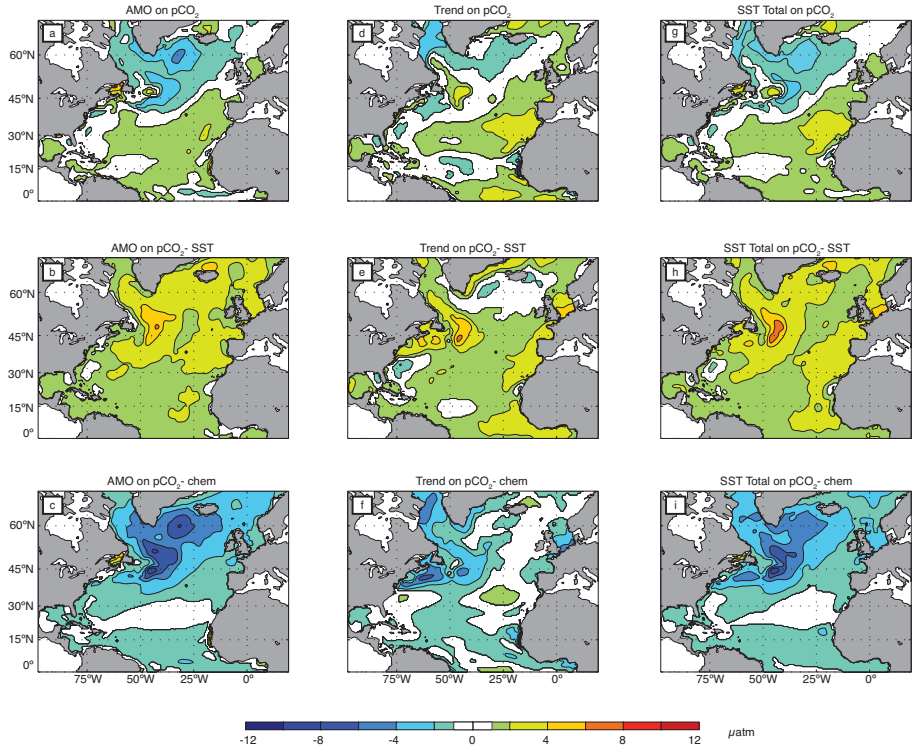

Figure 3. 121 month box-smoothed AMO regressed onto unsmoothed, monthly **(a)** pCO_2, **(b)** pCO_2-SST, **(c)** pCO_2-chem. SST Trend regressed onto **(d)** pCO_2, **(e)** pCO_2-SST, **(f)** pCO_2-chem. NASST (AMO + SST Trend) regressed onto **(g)** pCO_2, **(h)** pCO_2-SST, **(i)** pCO_2-chem. Regressions calculated from 1953 through 2005. Values < 0.5 and > -0.5 µatm are whited out to highlight regions experiencing the most substantial changes.

BGD
12, 15223–15244, 2015

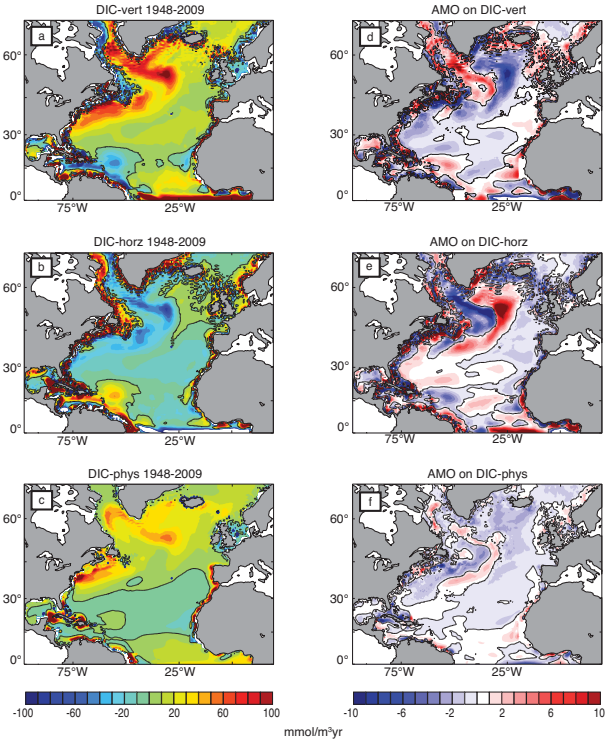

Figure 4. DIC diagnostics. Left column: 1948–2009 Mean **(a)** DIC-vertical, **(b)** DIC-horizontal, **(c)** DIC-physical where DIC-physical is the sum of DIC-vertical and DIC-horizontal. Right column: AMO regressed onto **(d)** DIC-vertical, **(e)** DIC-horizontal, **(f)** DIC-physical. Unit: $\mathrm{mmol\,m^{-3}\,yr^{-1}}$.

BGD
12, 15223–15244, 2015

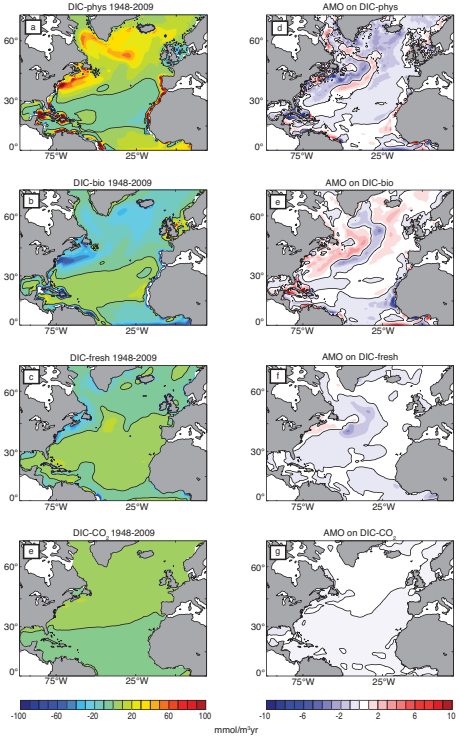

Figure 5. DIC diagnostics. Left column: 1948–2009 Mean **(a)** DIC-physical, **(b)** DIC-bio, **(c)** DIC-fresh, **(d)** DIC-CO_2 flux. Right column: AMO regressed onto **(e)** DIC-physical, **(f)** DIC-bio, **(g)** DIC-fresh, **(h)** DIC-CO_2 flux. Unit: mmol m^{-3} yr^{-1}.

BGD
12, 15223–15244, 2015